Physics of Plasmas

Numerical turbulence simulations of intermittent fluctuations in the scrape-off layer of magnetized plasmas

Cite as: Phys. Plasmas **28**, 072301 (2021); https://doi.org/10.1063/5.0047566
Submitted: 15 February 2021 • Accepted: 10 June 2021 • Published Online: 01 July 2021

G. Decristoforo, A. Theodorsen, J. Omotani, et al.

Physics of Plasmas ARTICLE scitation.org/journal/php

Numerical turbulence simulations of intermittent fluctuations in the scrape-off layer of magnetized plasmas

Cite as: Phys. Plasmas **28**, 072301 (2021); doi: 10.1063/5.0047566
Submitted: 15 February 2021 · Accepted: 10 June 2021 ·
Published Online: 1 July 2021

G. Decristoforo,[1,a)] A. Theodorsen,[1] J. Omotani,[2] T. Nicholas,[3] and O. E. Garcia[1]

AFFILIATIONS

[1]Department of Physics and Technology, UiT The Arctic University of Norway, NO-9037 Tromsø, Norway
[2]United Kingdom Atomic Energy Authority, Culham Centre for Fusion Energy, Culham Science Centre, Abingdon, Oxon OX14 3DB, United Kingdom
[3]Department of Physics, York Plasma Institute, University of York, Heslington, York YO10 5DD, United Kingdom

[a)]Author to whom correspondence should be addressed: gregor.decristoforo@uit.no

ABSTRACT

Intermittent fluctuations in the boundary of magnetically confined plasmas are investigated by numerical turbulence simulations of a reduced fluid model describing the evolution of the plasma density and electric drift vorticity in the two-dimensional plane perpendicular to the magnetic field. Two different cases are considered: one describing resistive drift waves in the edge region and another including only the interchange instability due to unfavorable magnetic field curvature in the scrape-off layer. Analysis of long data time series obtained by single-point recordings is compared to predictions of a stochastic model describing the plasma fluctuations as a superposition of uncorrelated pulses. For both cases investigated, the radial particle density profile in the scrape-off layer is exponential with a radially constant scale length. The probability density function for the particle density fluctuations in the far scrape-off layer has an exponential tail. Radial motion of blob-like structures leads to large-amplitude bursts with an exponential distribution of peak amplitudes and the waiting times between them. The average burst shape is well described by a two-sided exponential function. The frequency power spectral density of the particle density is simply that of the average burst shape and is the same for all radial positions in the scrape-off layer. The fluctuation statistics obtained from the numerical simulations are in excellent agreement with recent experimental measurements on magnetically confined plasmas. The statistical framework defines a new validation metric for boundary turbulence simulations.

I. INTRODUCTION

At the boundary of magnetically confined plasma, turbulent transport of particles and heat in the outermost region enhances plasma interactions with the material surfaces. This can become a serious issue for future fusion experiments and reactors.[1–3] A complete description of the physical mechanisms underlying the cross field plasma and heat transport in the scrape-off layer (SOL) and its effects on plasma–wall interactions is necessary if reliable predictions for reactor relevant devices are to be obtained. Unfortunately, such an understanding is at present still not fully achieved and predictions and extrapolations are often based on empirical scaling laws or highly simplified transport modeling with limited theoretical foundation.[3–5]

Fluctuations and turbulent motions in the boundary region of magnetized plasmas have been extensively investigated both experimentally and theoretically. It is recognized that in the SOL, radial motion of blob-like filament structures is the dominant mechanism for cross field transport of particles and heat.[6–9] This leads to broadening and flattening of radial profiles and high average particle density in the SOL that increases plasma–wall interactions.[10–23] Experimental measurements using Langmuir probes and gas puff imaging have revealed highly intermittent fluctuations of the particle density in the far SOL. Interestingly, measurements across a variety of magnetic geometries, including conventional tokamaks, spherical tokamaks, reversed field pinches, and stellarators have shown similar fluctuation characteristics.[24–27] Recent statistical analysis of exceptionally long fluctuation data time series from several tokamak devices has shown that the fluctuations are well described as a superposition of uncorrelated exponential pulses with fixed duration, arriving according to a Poisson process and with exponentially distributed pulse amplitudes.[28–42] A statistical framework based on filtered Poisson

processes has proven an accurate description of both average radial profiles and fluctuations in the boundary of magnetically confined plasma.[43–53]

So far, this stochastic model has not been utilized to analyze fluctuation data from numerical turbulence simulations of the boundary region of magnetized plasmas. In order to obtain statistically significant results, long simulation data time series or a large ensemble is required, equivalent to several hundred milliseconds in experiments with medium-sized magnetically confined plasma. Since most turbulence simulation studies have been focused on the dynamics of individual blob structures or on the effects of specific physical mechanisms on turbulence and transport, the simulations have likely not produced time series data of sufficient duration in order to analyze them in the same manner as the experimental measurements.[28–42] In this paper, we present the first results from applying the same statistical framework on numerical simulation data as has recently been done on experimental measurements. By using a simplified turbulence model describing the fluctuations in the two-dimensional plane perpendicular to the magnetic field, we have obtained data time series sufficiently long to allow unambiguous identification of the fluctuation statistics. The main goal of this study is to clarify these statistical properties and compare them with that found from experimental measurements. This is considered as an essential step toward validation of turbulence simulation codes.[54–56]

A recent analysis of fluctuation data time series obtained from numerical simulations of turbulent Rayleigh–Bénard-convection in two dimensions has given some illuminating results.[57] This model has frequently been used as a simplified description of the non-linear interchange dynamics in the SOL of magnetically confined plasmas.[58–66] In Ref. 57, it was found that the fluctuation time series is well described as a superposition of Lorentzian pulses, resulting in an exponential frequency power spectral density. In the present study, more sophisticated models for SOL turbulence are investigated, including sheath dissipation due to losses along magnetic field lines intersecting material surfaces as well as drift wave dynamics in the edge region.[67–83] The resulting far SOL data time series is shown to be dominated by large-amplitude bursts with a two-sided exponential pulse shape and fluctuation statistics that compare favorably with those found in experimental measurements.[28–42]

In this contribution, we present a detailed statistical analysis of fluctuation data time series from numerical simulations of a two-dimensional reduced fluid model describing the evolution of the electron density and electric drift vorticity. The paper is structured as follows. The reduced fluid model equations, normalization, and parameters are discussed in Sec. II. A brief introduction to the stochastic model is also presented here. We present the results for the time-averaged profiles and probability densities in Sec. III and for the fluctuation statistics in Sec. IV. A discussion of the results and the conclusions is finally presented in Sec. V.

II. MODEL EQUATIONS

The reduced fluid model investigated here is motivated by previous simulation studies performed by Sarazin *et al.*,[69–71] Garcia *et al.*,[72–74] Myra *et al.*,[75–77] Bisai *et al.*,[78–80] and Nielsen *et al.*[81–83] One particular case of the model is equivalent to that used in Ref. 71 and simulates SOL conditions in the entire simulation domain where a particle source is located close to the inner boundary. The particle density profile results from a balance between the plasma source, the sheath dissipation, and the radial transport due to the interchange instability. Another case of the model is similar to that used in Ref. 79 and features a simulation domain separating an edge region corresponding to plasma dynamics on closed magnetic flux surfaces and a SOL region where sheath dissipation balances the interchange drive. The source term is located in the plasma edge region where parallel resistivity gives rise to unstable drift waves. Despite these two fundamentally different descriptions of the primary instability mechanism underlying the SOL turbulence, the resulting fluctuations are remarkably similar to those will be shown in the following.

Similar to many previous investigations, we use two-field fluid model equations describing the plasma evolution in the edge and SOL regions for a quasi-neutral plasma, neglecting electron inertia and assuming for simplicity isothermal electrons and negligibly small ion temperature.[69–71,78–80] These simplifications lead to a highly efficient numerical implementation of the model equations, allowing us to obtain simulation data time series of unprecedented duration that is suitable for detailed statistical analysis.

We choose a slab geometry where x refers to the radial direction and y to the binormal or poloidal direction. The reduced electron continuity and electron drift vorticity equations are given as

$$\frac{\mathrm{d}n}{\mathrm{d}t} + g\left(\frac{\partial n}{\partial y} - n\frac{\partial \phi}{\partial y}\right) = \Sigma_n + D_\perp \nabla_\perp^2 n + \langle \nabla_\parallel J_{\parallel \mathrm{e}} \rangle_\parallel, \tag{1a}$$

$$\frac{\mathrm{d}\nabla_\perp^2 \phi}{\mathrm{d}t} + \frac{g}{n}\frac{\partial n}{\partial y} = \nu_\perp \nabla_\perp^4 \phi + \left\langle \frac{1}{n}\nabla_\parallel J_\parallel \right\rangle_\parallel, \tag{1b}$$

where n represents the normalized electron density, ϕ is the normalized electric potential, g is normalized effective gravity (that is, drive from unfavorable magnetic curvature), Σ_n is the plasma source term, and $D_\perp$ and $\nu_\perp$ are the normalized particle and vorticity diffusion coefficients. We use the standard Bohm normalization as previously used and discussed in Refs. 67–80, that is, spatial units are normalized by the ion sound Larmor radius ρ_s, temporal units by the ion gyration frequency $\Omega_\mathrm{i} = eB/m_\mathrm{i}$, particle density n by a characteristic density n_0, electrostatic potential ϕ by T_0/e, where T_0 is the electron temperature, parallel electric current, $J_\parallel$ and electron current $J_{\parallel \mathrm{e}}$ by en_0c_s, where $c_s = (T_0/m_\mathrm{i})^{1/2}$ is the cold ion sound speed, g is given by $2\rho_\mathrm{s}/R$, where R is the major radius at the low-field side SOL, and $D_\perp$ and $\nu_\perp$ are normalized by $1/\rho_\mathrm{s}^2\Omega_\mathrm{i}$. In addition, we have the advective derivative $\mathrm{d}/\mathrm{d}t = \partial/\partial t + \mathbf{V}_\mathrm{E}\cdot\nabla_\perp$, where $\mathbf{V}_\mathrm{E} = \hat{\mathbf{z}}\times\nabla\phi$ is the electric drift. The plasma source term is given by $\Sigma_n(x) = \Sigma_0\ \exp(-(x-x_0)^2/\lambda_\mathrm{s}^2)$, where Σ_0 is the maximum amplitude of the source normalized by $1/n_0\Omega_\mathrm{i}$, x_0 is the source location, and λ_s is the e-folding length for the source.

Equations (1a) and (1b) are averaged along the magnetic field lines, with the contribution from the normalized parallel electron $J_{\parallel \mathrm{e}}$ and total plasma currents $J_\parallel$ in the sheath connected regime given by

$$\langle \nabla_\parallel J_{\parallel \mathrm{e}} \rangle_\parallel = -\sigma n\ \exp(\Lambda - \phi) + \chi(\hat{\phi} - \hat{n}), \tag{2a}$$

$$\left\langle \frac{1}{n}\nabla_\parallel J_\parallel \right\rangle_\parallel = \sigma[1 - \exp(\Lambda - \phi)] + \chi(\hat{\phi} - \hat{n}). \tag{2b}$$

Here, Λ is the sheath potential, σ the normalized sheath dissipation coefficient, and χ the normalized parallel plasma conductivity. Like in

several previous investigations, these parameters are taken to be a function of the radial position in the boundary region.[72–83] In particular, the sheath dissipation coefficient σ is finite in the SOL region ($x > x_{SOL}$) and vanishes in the edge ($x < x_{SOL}$), which corresponds to the region with closed magnetic flux surfaces. These two regions are connected with a smooth function due to numerical reasons, that is, $\sigma(x) = \sigma_0\{1 + \tanh[w(x - x_{SOL})]\}/2$. The slope of this function is determined by the width parameter w, which is set to $w = 25/32$. Similarly, the plasma conductivity χ is neglected in the SOL and is finite in the edge region, that is, $\chi(x) = \chi_0(1 - \{1 + \tanh[w(x - x_{SOL})]\}/2)$. Here, $\sigma_0 = \rho_s/L_c$ with L_c the parallel connection length and $\chi_0 = (\rho_s k_\parallel)^2(m_i/m_e)(\Omega_i/\nu_{ei})$, where $k_\parallel$ is the dominant parallel wave number for the edge region drift waves and ν_{ei} stands for the collision frequency between electrons and ions. The simulation domain is sketched in Fig. 1, showing the location of the plasma source and the separation between the edge and SOL regions. Furthermore, the spatially fluctuating electron density $\hat{n}$ and plasma potential $\hat{\phi}$ are defined as $\hat{n} = n - \langle n\rangle_y$ and $\hat{\phi} = \phi - \langle\phi\rangle_y$, where $\langle\cdot\rangle_y$ refers to the flux surface average. This leads to the final reduced electron continuity and electric drift vorticity equations,

$$\frac{dn}{dt} + g\left(\frac{\partial n}{\partial y} - n\frac{\partial\phi}{\partial y}\right) = \Sigma_n(x) + D_\perp\nabla_\perp^2 n - \sigma(x)\, n\, \exp(\Lambda - \phi) + \chi(x)(\hat{\phi} - \hat{n}), \tag{3a}$$

$$\frac{d\nabla_\perp^2\phi}{dt} + \frac{g}{n}\frac{\partial n}{\partial y} = \nu_\perp\nabla_\perp^4\phi + \sigma(x)[1 - \exp(\Lambda - \phi)] + \chi(x)(\hat{\phi} - \hat{n}). \tag{3b}$$

In the following, we present results from numerical simulations of this model for two different cases. In the first case, the domain is split into two regions, effectively the edge and the SOL regions, by taking $x_{SOL} = 50$. In the second case, a pure SOL plasma is considered with $x_{SOL} = 0$, and thus, plasma conductivity χ is not present in the simulation domain.

The input parameters have been chosen to be similar to that used in previous publications based on this model.[79] For all runs presented here, the simulation domain lengths are chosen to be $L_x = 200$ and $L_y = 100$, with the border between the edge and the SOL at $x_{SOL} = 50$ for the two-region case. It has been verified that a change in the size of the simulation domain does not influence the fluctuation statistics. The simulation code is implemented in BOUT++[84] utilizing the STORM branch,[85] which uses a finite difference scheme in the x-direction and a spectral scheme in the y-direction. Time integration is performed with the PVODE solver.[86] We use a resolution of 512×256 grid points for all runs. We further take $D_\perp = \nu_\perp = 10^{-2}$, $g = 10^{-3}$, $\chi_0 = 6 \times 10^{-4}$, $\Sigma_0 = 11/2000$, $\sigma_0 = 5 \times 10^{-4}$, and $\Lambda = 0.5\ln(2\pi m_i/m_e)$ with deuterium ions, $x_0 = 20$ and $\lambda_s = 10$. We apply periodic boundary conditions in the poloidal direction and zero gradient boundary conditions in the radial direction for both the electron density and vorticity fields. For the plasma potential, we use zero gradient boundary conditions at the outer boundary and fixed boundary conditions $\phi(x = 0) = 0$ at the inner boundary.

During the simulations, the plasma parameters at nine different radial positions in the simulation domain are recorded with a sampling frequency of one in normalized time units. The location of these probes is presented in Fig. 1. This corresponds to single-point measurements in the experiments, and the simulation data will be analyzed in the same manner as has previously been done for experimental measurement data. The contour plots of the electron density in both simulation cases presented in Fig. 2 show several blob-like structures with the familiar mushroom-shape typical for strongly non-linear interchange motions.[65]

Time series of the plasma parameters with a duration of 2×10^6 time units has been obtained under statistically stationary conditions, that is, excluding initial transients in the turbulence simulations. Ten simulation runs with this duration time and different random initial conditions are performed for the two-region model and seven for the one region model. The fluctuation statistics to be presented in Sec. IV

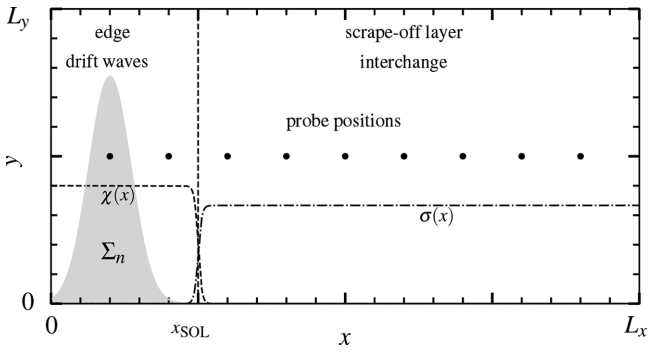

FIG. 1. Schematic illustration of the simulation domain for the $x_{SOL} = 50$ case. The position of the plasma source term (gray shaded) and the border between edge and SOL (dashed vertical line) are indicated. The radial variation of the sheath dissipation and parallel conductivity coefficients is also shown.

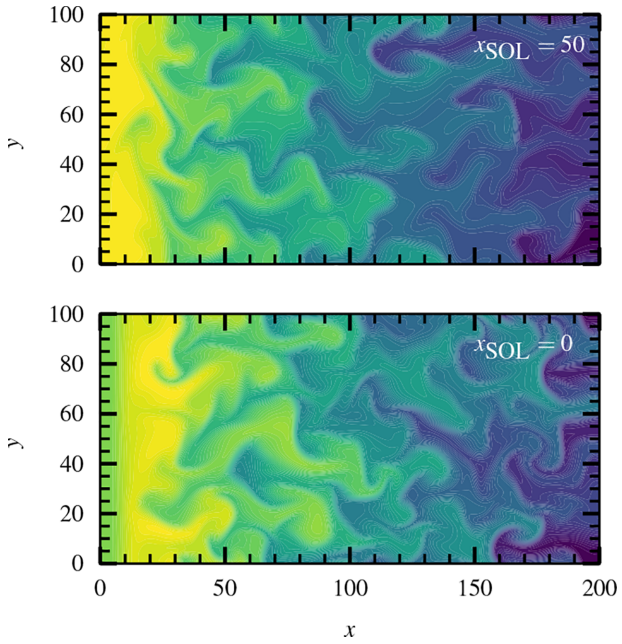

FIG. 2. Contour plots of $\log(n)$ in the turbulent state for the $x_{SOL} = 0$ and $x_{SOL} = 50$ cases showing the presence of mushroom-shaped blob-like structures in the SOL.

are based on these ensembles of simulation data. In the following analysis, we will frequently consider plasma parameters normalized such as to have vanishing mean and unit standard deviation, for example. For the electron density, we define

$$\tilde{n} = \frac{n - \langle n \rangle}{n_{\mathrm{rms}}}, \tag{4}$$

where the angular brackets denote a time average and n_{rms} is the root mean square value calculated from the time series. A short part of the normalized electron density time series is presented in Fig. 3 for both simulation cases, showing frequent appearance of large-amplitude bursts due to the high density blob-like structures moving radially outwards. The radial variation of the lowest order moments of these fluctuations is presented and discussed in Sec. III. The electron density time series is compared to the radial velocity v_x and the radial particle flux $\Gamma = nv_x$ in Fig. 4 for the $x_{\mathrm{SOL}} = 0$ simulation. All quantities are normalized according to Eq. (4). It is shown that large-amplitude events in the particle density are correlated with positive radial velocities resulting in high levels of radial particle transport. The same observations are made for the $x_{\mathrm{SOL}} = 50$ simulation (not presented here).

In the following, the numerical simulation data will be compared to predictions of a stochastic model, which describes the fluctuations as a superposition of uncorrelated pulses with fixed shape and constant duration. This is written as[43–53]

$$\Psi_K(t) = \sum_{k=1}^{K(T)} A_k \psi\left(\frac{t - t_k}{\tau_{\mathrm{d}}}\right), \tag{5}$$

where ψ is the pulse function, τd is the pulse duration time, $K(T)$ is the number of pulses for a realization of duration T, and for the event labeled k the pulse amplitude is A_k and the arrival time t_k. The mean value of the random variable Ψ_K is $\langle \Psi \rangle = (\tau_{\mathrm{d}}/\tau_{\mathrm{w}})\langle A \rangle$, where $\langle A \rangle$ is the average pulse amplitude and τw is the average pulse waiting time. We will assume pulses arriving according to a Poisson process, which implies independent and exponentially distributed waiting times and independent arrival times uniformly distributed on the realization. We further assume independently and exponentially distributed amplitudes, $P_A(A) = \exp(-A/\langle A \rangle)/\langle A \rangle$, and we will consider the case of a two-sided exponential pulse function,[50]

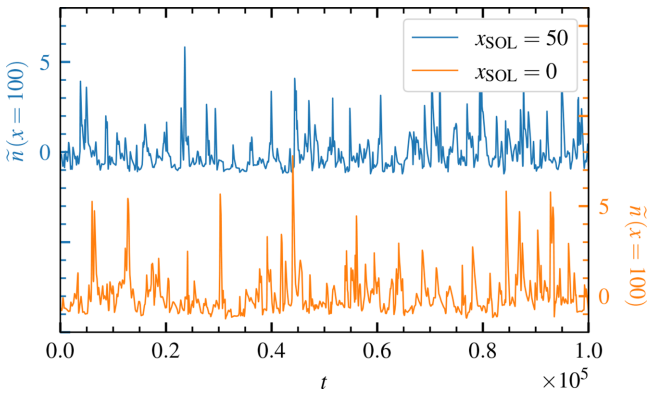

FIG. 3. A short part of the normalized electron density time series recorded at $x = 100$ for the $x_{\mathrm{SOL}} = 0$ and $x_{\mathrm{SOL}} = 50$ simulation cases.

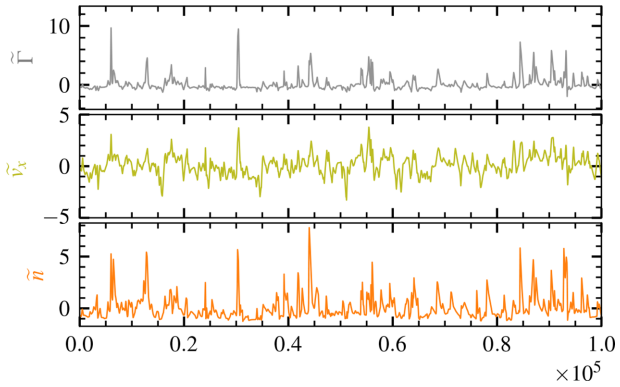

FIG. 4. Normalized electron density time series compared to the normalized radial velocity and normalized radial particle flux recorded at $x = 100$ for the $x_{\mathrm{SOL}} = 0$ simulation case.

$$\psi(\theta; \lambda) = \begin{cases} \exp(\theta/\lambda), & \theta < 0, \\ \exp[-\theta/(1-\lambda)], & \theta \geq 0, \end{cases} \tag{6}$$

where the pulse asymmetry parameter λ is restricted to the range $0 < \lambda < 1$. For $\lambda < 1/2$, the pulse rise time is faster than the decay time, while the pulse shape is symmetric in the case $\lambda = 1/2$. The frequency power spectral density for this process is just the spectrum of the pulse function,[50]

$$\Omega_{\tilde{\Psi}}(\omega) = \frac{2\tau_{\mathrm{d}}}{\left[1 + (1-\lambda)^2(\tau_{\mathrm{d}}\omega)^2\right]\left[1 + \lambda^2(\tau_{\mathrm{d}}\omega)^2\right]}, \tag{7}$$

where ω is the angular frequency. Note that the power spectral density of $\tilde{\Psi}$ is independent of the amplitude distribution. From this, it follows that the frequency power spectral density can be used to estimate the pulse parameters τd and λ, which will be done in the following analysis of the numerical simulations.

The stationary probability density function (PDF) for the random variable Ψ_K can be shown to be a gamma distribution,[53]

$$\langle \Psi \rangle P_\Psi(\Psi) = \frac{\gamma}{\Gamma(\gamma)}\left(\frac{\gamma\Psi}{\langle \Psi \rangle}\right)^{\gamma-1} \exp\left(\frac{\gamma\Psi}{\langle \Psi \rangle}\right), \tag{8}$$

with shape parameter $\gamma = \tau_{\mathrm{d}}/\tau_{\mathrm{w}}$, that is, the ratio of the pulse duration and the average pulse waiting time τw. This parameter describes the degree of pulse overlap, which determines the level of intermittency in the process. From the gamma distribution, it follows that the skewness moment is $S_\Psi = \langle(\Psi - \langle \Psi \rangle)^3\rangle/\Psi_{\mathrm{rms}}^3 = 2/\gamma^{1/2}$ and the flatness moment is $F_\Psi = \langle(\Psi - \langle \Psi \rangle)^4\rangle/\Psi_{\mathrm{rms}}^4 = 3 + 6/\gamma$. Accordingly, there is a parabolic relationship between these moments given by $F_\Psi = 3 + 3S_\Psi^2/2$. For strong pulse overlap and large γ, the probability density function approaches a normal distribution and the skewness S_Ψ and excess flatness $F_\Psi - 3$ moments vanish.

III. PROFILES AND DISTRIBUTIONS

The time-averaged electron density profiles in the turbulence simulations are presented in Fig. 5. Since the $x_{\mathrm{SOL}} = 50$ case does not include any sheath dissipation in the edge region, the average density is higher here than for the $x_{\mathrm{SOL}} = 0$ case. Throughout the SOL region,

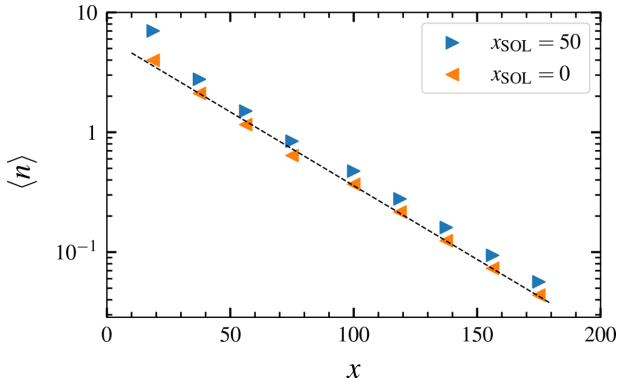

FIG. 5. Time-averaged electron density profile for the $x_{SOL} = 0$ and $x_{SOL} = 50$ cases. The broken line is the best fit of an exponential function with a scale length of 35.5.

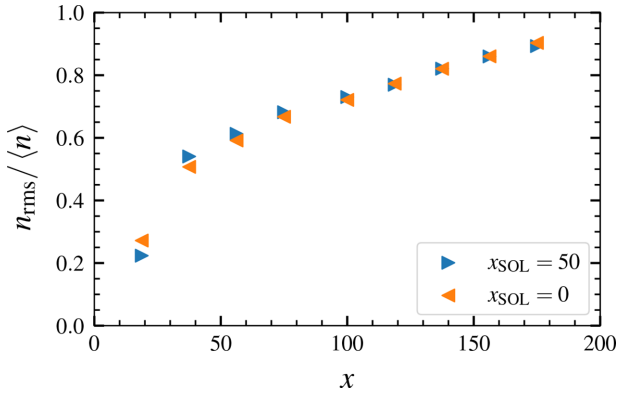

FIG. 6. The relative fluctuation level of the electron density at different positions in the SOL for the $x_{SOL} = 0$ and $x_{SOL} = 50$ cases.

we observe that the electron density decreases exponentially with a radially constant scale length of 35.5. This is to be compared with the equilibrium SOL profile scale length in the absence of turbulence given by $\sqrt{D_\perp/\sigma_0} = \sqrt{20}$ for the simulation parameters used here.

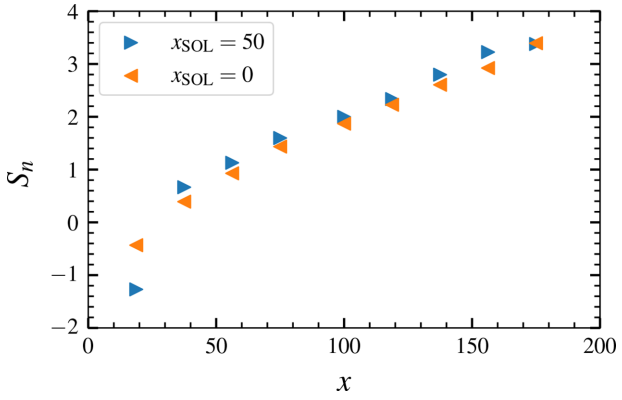

FIG. 7. Skewness of the electron density fluctuations at different radial positions for the $x_{SOL} = 0$ and $x_{SOL} = 50$ cases.

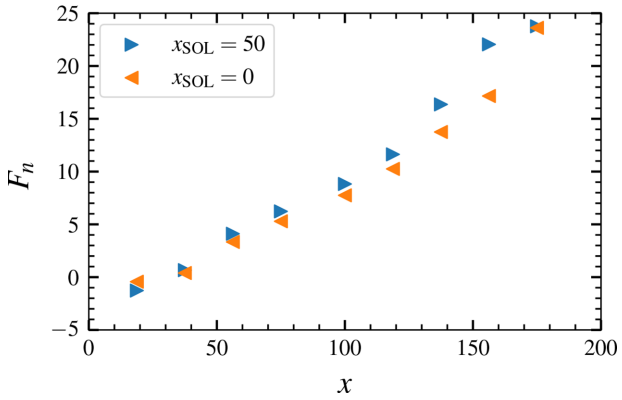

FIG. 8. Flatness of the electron density fluctuations at different radial positions for the $x_{SOL} = 0$ and $x_{SOL} = 50$ cases.

Interestingly, both the scale length and the absolute density are very similar for the two simulation cases investigated. We further show the relative fluctuation level at different radial positions for both cases in Fig. 6. The normalized fluctuation level is very high, increases radially outwards as the time-averaged density decreases faster than the absolute fluctuation level, and is roughly similar for the two simulation cases.

The radial variation of the skewness and flatness moments of the electron density fluctuations is presented in Figs. 7 and 8, respectively. From these figures, it is clear that the intermittency of the fluctuations increases radially outwards in the SOL, qualitatively similar for the $x_{SOL} = 0$ and $x_{SOL} = 50$ cases. By plotting the flatness moment vs the skewness, presented in Fig. 9, it is seen that for both simulation cases there is a nearly parabolic relationship between these higher order moments. The moments at $x = 18.75$ are not shown in Fig. 9 since they are measured close to the maximum amplitude of the source term. Such a parabolic relationship is predicted by the stochastic model describing the fluctuations as a superposition of uncorrelated pulses,[43–46] which can be related to blob-like structures moving radially outwards in the SOL as seen in Fig. 2.

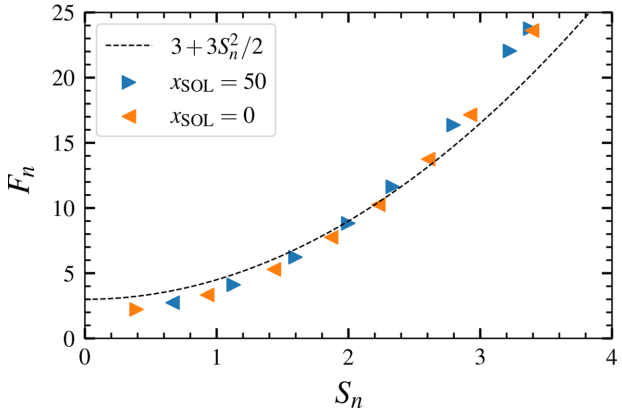

FIG. 9. Flatness plotted vs skewness for the electron density fluctuations in the SOL. The broken line shows the parabolic relationship $F_n = 3 + 3S_n^2/2$ for comparison.

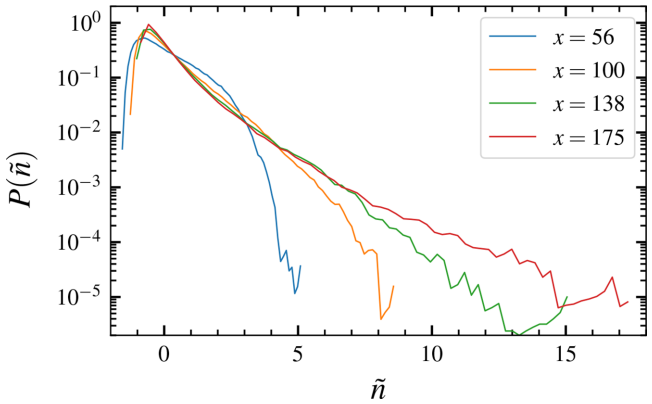

FIG. 10. Probability density functions of the normalized electron density recorded at different radial positions for the $x_{SOL} = 0$ case.

The PDFs for the normalized electron density fluctuations at different radial positions are presented in Figs. 10 and 11 for the $x_{SOL} = 0$ and $x_{SOL} = 50$ cases, respectively. The PDFs change from a narrow and nearly symmetric distribution in the edge/near SOL region to a distribution with an exponential tail for large fluctuation amplitudes in the far SOL. In Fig. 12, we further compare the PDFs of the electron density time series recorded in the far SOL at $x = 100$ for both simulation cases with a gamma distribution with a shape parameter of 1.4. Such a gamma distribution is predicted by the stochastic model describing the fluctuations as a superposition of uncorrelated exponential pulses. The gamma distribution is clearly an excellent description of the PDF for the electron density fluctuations in the simulations. A similar change in the shape of the PDF radially outwards in the SOL has also been reported from previous turbulence simulations.[72–74]

IV. FLUCTUATION STATISTICS

In this section, we present a detailed analysis of the electron density fluctuations recorded at $x = 100$. In order to reveal the typical shape of large-amplitude bursts in the time series, a conditional averaging method which allows for overlapping events is applied. This

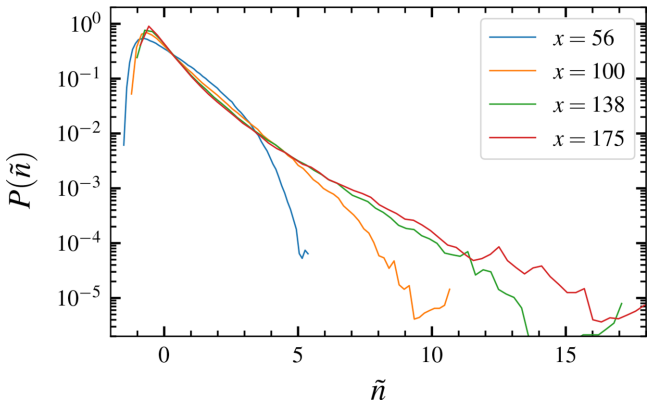

FIG. 11. Probability density functions of the normalized electron density recorded at different radial positions for the $x_{SOL} = 50$ case.

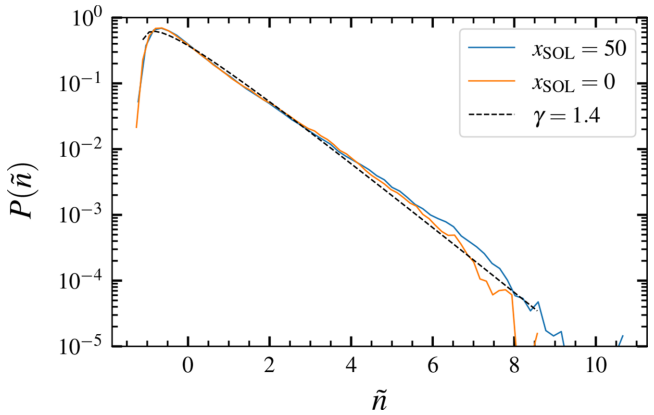

FIG. 12. Probability density functions of the normalized electron density recorded at $x = 100$ for both simulations cases compared to a gamma distribution with shape parameter $\gamma = 1.4$ shown with the dashed black line.

identifies a total of 3128 conditional events with peak amplitudes larger than 2.5 times the root mean square value above the mean for the $x_{SOL} = 50$ case and 1701 conditional events for the $x_{SOL} = 0$ case. The average burst structures are presented in Fig. 13 and show an asymmetric shape with a fast rise and a slower decay. The burst shape is compared to an asymmetric, two-sided exponential function given by Eq. (6) with duration time $\tau_d = 300$ and asymmetry parameter $\lambda = 0.2$. The conditional burst shape is shown with semilogarithmic axes in the inset in Fig. 13, showing that the decay of the conditional pulse shape is approximately exponential. However, the two-sided exponential function obviously fails to describe the smooth peak of the average burst shape in the simulations. As shown for short time lags in Fig. 13, this is better described using a skewed Lorentzian pulse as a fit function with duration 80 and skewness parameter 1 for the $x_{SOL} = 50$ case.[87–90] The slightly elevated tails of the conditional burst shape are likely due to finite pulse overlap in the turbulence simulations.

The frequency power spectral density due to a superposition of uncorrelated exponential pulses is compared to the simulation data of

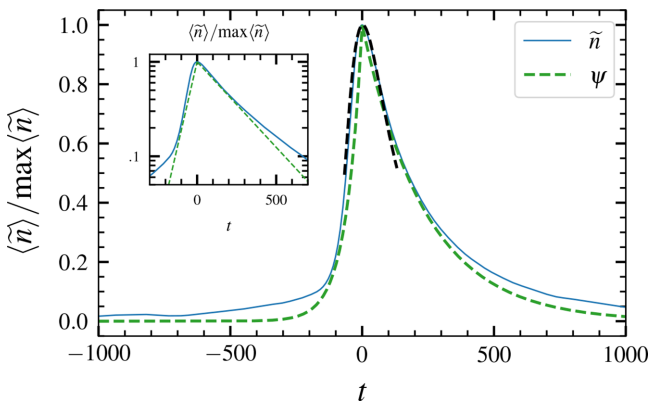

FIG. 13. Conditionally averaged burst shape at $x = 100$ of the $x_{SOL} = 50$ case (full blue line) compared to a two-sided exponential pulse (dashed green line), as well as a skewed Lorentzian pulse for short time lags (dashed black line). The conditional average is normalized by its peak amplitude.

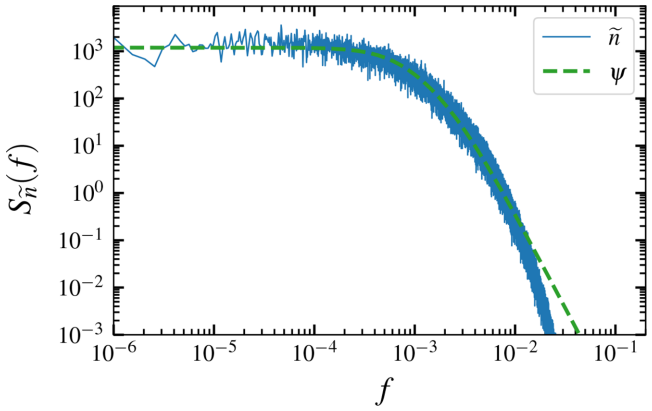

FIG. 14. Frequency power spectral density of the electron density fluctuations recorded at $x = 100$ for the $x_{SOL} = 50$ case (full blue line). This is compared to the predictions of a stochastic model describing the fluctuations as a superposition of uncorrelated, two-sided exponential pulses with duration time $\tau_d = 300$, and asymmetry parameter $\lambda = 0.2$ (dashed green line).

the electron density fluctuations recorded at $x = 100$ in Fig. 14 for the $x_{SOL} = 50$ case. It is shown that the spectrum gives excellent agreement for high powers and low frequencies. Similar results for conditional averaging and frequency power spectra are found for the case $x_{SOL} = 0$ but with slightly different pulse parameters.

The conditionally averaged burst shape is presented in Fig. 15 for different radial positions in the SOL for the $x_{SOL} = 50$ case. Here it is seen that the burst shape in the far SOL region is the same for all radial positions, despite the fact that the relative fluctuation amplitude increases radially outwards. Accordingly, as predicted by the stochastic model, the frequency power spectral density has the same shape for all these different radial positions, as is shown in Figs. 16 and 17 for both the one- and two-region cases. The spectra are well described by that of a two-sided exponential pulse function, shown by the dashed black line in the figures.

Restricting the peak amplitude of conditional events in the electron density to be within a range of 2–4, 4–6, and 6–8 times the rms value, the appropriately scaled conditional burst shapes are presented in Fig. 18. This reveals that the average burst shape and duration do

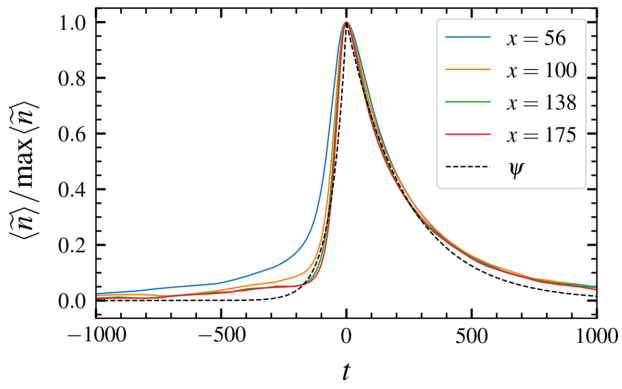

FIG. 15. Conditionally averaged burst shapes at different radial positions for the $x_{SOL} = 50$ case. The conditional averages are normalized by their peak amplitude.

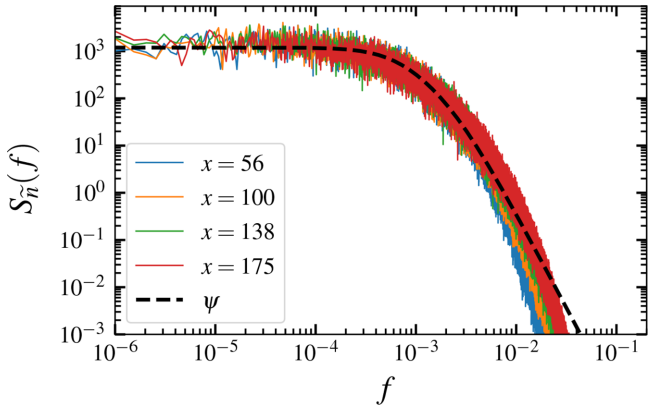

FIG. 16. Frequency power spectral densities of the electron density fluctuation recorded at different radial positions for the $x_{SOL} = 50$ model. The dashed line shows the spectrum due to a superposition of uncorrelated, two-sided exponential pulses with duration time τd.

not depend on the burst amplitude and are again well described by a two-sided exponential function except for the smooth peak. This supports the assumption of fixed pulse duration in the stochastic model describing the fluctuations as a superposition of pulses.

From the conditional averaging, we further obtain the peak amplitudes of conditional events and the waiting times between them. The PDFs of these are presented in Figs. 19 and 20, respectively. The distributions are similar for both simulation cases and are clearly well described by an exponential distribution as shown by the dashed black line in the plots. This is in agreement with the assumptions for the stochastic model presented in Sec. II. In particular, the exponential waiting time distribution supports the hypothesis that the events are uncorrelated and arrive according to a Poisson process.

V. DISCUSSION AND CONCLUSIONS

The abundant experimental evidence for universal statistical properties of fluctuations in the SOL of magnetically confined fusion

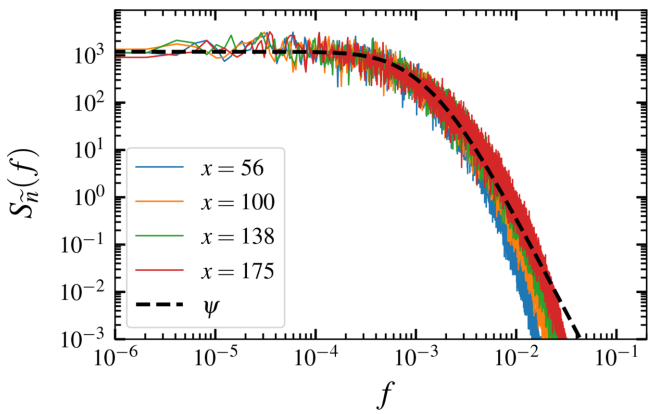

FIG. 17. Frequency power spectral densities of the electron density fluctuation recorded at different radial positions for the $x_{SOL} = 0$ model. The dashed line shows the spectrum due to a superposition of uncorrelated two-sided exponential pulses.

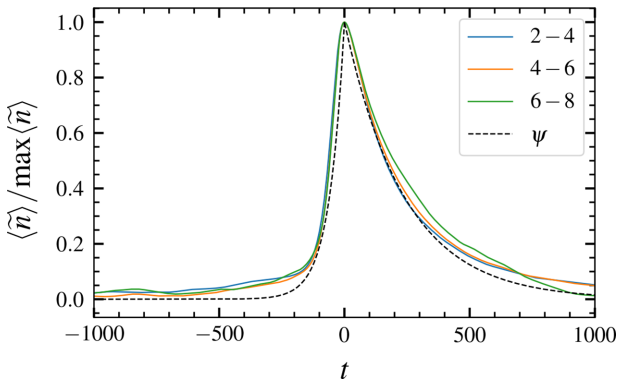

FIG. 18. Conditionally averaged burst shape at $x = 100$ of the $x_{SOL} = 50$ case for different conditional amplitude threshold intervals. The conditional averages are normalized by their peak amplitudes.

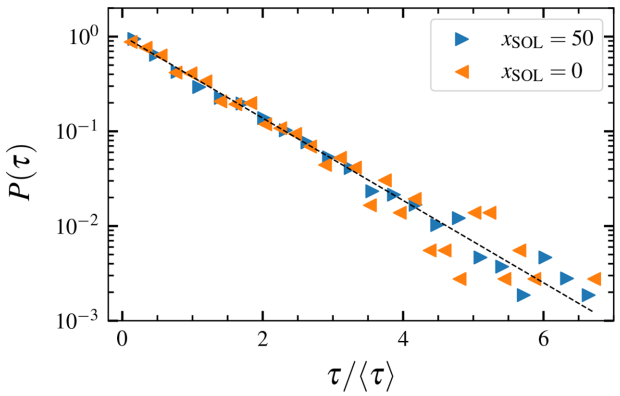

FIG. 20. Probability density functions of waiting times between consecutive large-amplitude burst in the electron density time series recorded at $x = 100$.

plasmas sets high requirements for validation of turbulence simulation codes for the boundary region.[54–56] In this context, we have examined the statistical properties of the electron density fluctuations in the SOL by numerical simulations of plasma turbulence in the two-dimensional plane perpendicular to the magnetic field. Two model cases have been considered: one describing resistive drift waves in the edge region and another including only the interchange instability due to unfavorable magnetic field curvature. For both cases, mushroom-shaped blob-like structures move radially outwards, resulting in large-amplitude fluctuations and high average particle densities in the SOL. The numerical simulations show that the time-averaged radial profile decreases exponentially with radial distance into the SOL with the same characteristic length scale for both simulation cases. Moreover, the fluctuation statistics in the SOL are the same for both cases. This is despite the different linear instability mechanisms driving the fluctuations in the edge/near SOL region in the two simulation cases. It appears that any drift-ordered instability mechanism will lead to formation of filament structures when coupled to a SOL region with unfavorable magnetic field curvature.

According to a stochastic model describing the profile as due to radial motion of filament structures, the profile scale length is given by the product of the radial filament velocity and the parallel transit time.[46–48] This suggests that typical filament velocities are the same in both simulation cases. Future work will investigate the distribution of filament sizes and velocities by analysis of the velocity fluctuations and applying a blob tracking algorithm as described in Ref. 91.

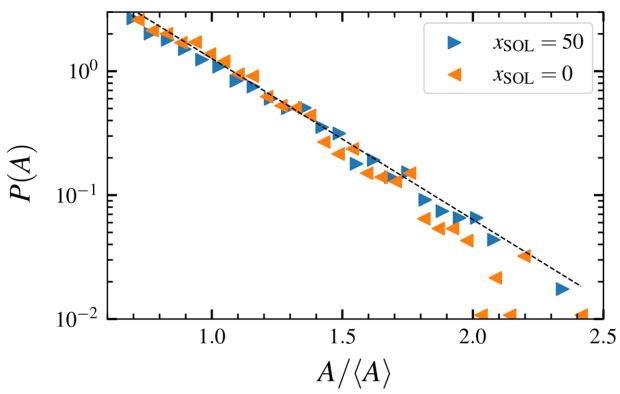

FIG. 19. Probability density functions of conditional burst amplitudes of the electron density time series recorded at $x = 100$.

The relative fluctuation level increases radially outwards, nearly reaching unity in the far SOL for the plasma parameters investigated here. Similarly, the skewness and flatness moments also increase into the SOL, and these higher order moments closely follow a quadratic dependence as predicted by the stochastic model describing the fluctuations as a superposition of uncorrelated pulses. The PDF of the electron density fluctuations changes from a nearly Gaussian distribution in the edge/near SOL region to a distribution with an exponential tail for large amplitudes in the far SOL. In the far SOL region, the PDFs are well described by a gamma distribution with the shape parameter given by the ratio of the pulse duration and average waiting time. The increase in this intermittency parameter with radial distance into the SOL suggests that only the most coherent and large-amplitude blob structures are able to move through the entire SOL region before they disperse and breakup due to secondary instabilities.

A conditional averaging analysis has revealed that the shape of large-amplitude bursts in single-point recordings in the far SOL is well described by a two-sided exponential pulse, as has previously been found in experimental measurements. Accordingly, the frequency power spectral density is well described by that of a two-sided exponential pulse for high powers and low frequencies. However, the high resolution and smoothness of the solution from the numerical computations imply that the burst structure has a rounded peak as opposed to the break point in experimental measurements due to their much lower sampling rate and additional measurement noise. The smooth peak is well described by a skewed Lorentzian pulse function. The frequency power spectral density therefore has an exponential decay for high frequencies and low powers with a slope that is given by the width of the narrow Lorentzian-shaped peak of large-amplitude fluctuations in the numerical simulations. In experimental measurements, this exponential tail in the spectrum may readily be masked by low sampling rates, limiting the highest frequencies resolved or by additive measurement noise, limiting the lowest power resolved.[49,50] The high frequency part of the power spectral density of the numerical

simulations therefore does not contradict experimental findings as these two counterparts cannot be directly compared.

In summary, it is here demonstrated that a simple but self-consistent model for turbulent fluctuations in the scrape-off layer reveals the same statistical properties of large-amplitude events as found in the experiments. This includes exponentially distributed pulse amplitudes and waiting times, the latter supporting the assumption of Poisson events.[28–33,36–40] The simulation data also agree with predictions of the stochastic model, namely, an exponential average profile, gamma-distributed fluctuation amplitudes, and a frequency power spectral density determined by the average shape of large-amplitude bursts. It is concluded that the filtered Poisson process, describing the fluctuations in single-point recordings as a superposition of uncorrelated pulses with fixed duration, is an excellent description of the SOL plasma fluctuations in the turbulence simulations investigated here.[43–53]

The simple turbulence model used in this study does not include finite ion temperature effects, X-point physics, parallel collisional conductivity in the scrape-off layer, or any effect of interactions with neutral particles. Numerous SOL turbulence models and codes are now being extended to include these features.[92–100] The statistical framework with superposition of filaments can be used for analysis and interpretation of simulation results in these more advanced models, similar to what has been done here and previously for experimental measurements. As such, this work sets a new standard for validation of turbulence simulation codes.[54–56]

ACKNOWLEDGMENTS

This work was supported by the UiT Aurora Centre Program, UiT The Arctic University of Norway (2020). A.T. was supported by a Tromsø Science Foundation Starting Grant under Grant No. 19–SG–AT. G.D. acknowledges the generous hospitality of the Culham Centre for Fusion Energy (CCFE) where parts of this work were conducted. Two supercomputers provided by the Norwegian Metacenter for Computational Science (NOTUR) were used for the computational work, the Fram and Stallo clusters at the University of Tromsø under Project No. nn9348k. The MARCONI supercomputer was used for parts of the computational work under the Project No. FUA34–SOLBOUT4. The storm2d project has been used as a template for the presented physical models. This work was funded in part by the RCUK Energy Programme (Grant No. EP/T012250/1) and the EPSRC Centre for Doctoral Training in the Science and Technology of Fusion Energy (Grant No. EP/L01663X/1), as well as an iCASE award from CCFE.

DATA AVAILABILITY

The data that support the findings of this study are available from the corresponding author upon reasonable request.

REFERENCES

[1]R. A. Pitts, J. P. Coad, D. P. Coster, G. Federici, W. Fundamenski, J. Horacek, K. Krieger, A. Kukushkin, J. Likonen, G. F. Matthews, M. Rubel, J. D. Strachan, and JET-EFDA Contributors, "Material erosion and migration in tokamaks," Plasma Phys. Controlled Fusion **47**, B303 (2005).

[2]B. Lipschultz, X. Bonnin, G. Counsell, A. Kallenbach, A. Kukushkin, K. Krieger, A. Leonard, A. Loarte, R. Neu, R. Pitts, T. Rognlien, J. Roth, C. Skinner, J. Terry, E. Tsitrone, D. Whyte, S. Zweben, N. Asakura, D. Coster, R. Doerner, R. Dux, G. Federici, M. Fenstermacher, W. Fundamenski, P. Ghendrih, A. Herrmann, J. Hu, S. Krasheninnikov, G. Kirnev, A. Kreter, V. Kurnaev, B. LaBombard, S. Lisgo, T. Nakano, N. Ohno, H. Pacher, J. Paley, Y. Pan, G. Pautasso, V. Philipps, V. Rohde, D. Rudakov, P. Stangeby, S. Takamura, T. Tanabe, Y. Yang, and S. Zhu, "Plasma-surface interaction, scrape-off layer and divertor physics: Implications for ITER," Nucl. Fusion **47**, 1189 (2007).

[3]A. Loarte, B. Lipschultz, A. Kukushkin, G. Matthews, P. Stangeby, N. Asakura, G. Counsell, G. Federici, A. Kallenbach, K. Krieger, A. Mahdavi, V. Philipps, D. Reiter, J. Roth, J. Strachan, D. Whyte, R. Doerner, T. Eich, W. Fundamenski, A. Herrmann, M. Fenstermacher, P. Ghendrih, M. Groth, A. Kirschner, S. Konoshima, B. LaBombard, P. Lang, A. Leonard, P. Monier-Garbet, R. Neu, H. Pacher, B. Pegourie, R. Pitts, S. Takamura, J. Terry, E. Tsitrone, and ITPA Scrape-off Layer and Divertor Physics Topical Group, "Chapter 4: Power and particle control," Nucl. Fusion **47**, S203 (2007).

[4]S. Wiesen, D. Reiter, V. Kotov, M. Baelmans, W. Dekeyser, A. S. Kukushkin, S. W. Lisgo, R. A. Pitts, V. Rozhansky, G. Saibene, I. Veselova, and S. Voskoboynikov, "The new SOLPS-ITER code package," J. Nucl. Mater. **463**, 480 (2015).

[5]X. Bonnin, W. Dekeyser, R. Pitts, D. Coster, S. Voskoboynikov, and S. Wiesen, "Presentation of the new SOLPS-ITER code package for tokamak plasma edge modelling," Plasma Fusion Res. **11**, 1403102 (2016).

[6]D. A. D'Ippolito, J. R. Myra, S. I. Krasheninnikov, G. Q. Yu, and A. Y. Pigarov, "Blob transport in the tokamak scrape-off-layer," Contrib. Plasma Phys. **44**, 205 (2004).

[7]S. I. Krasheninnikov, D. A. D'Ippolito, and J. R. Myra, "Recent theoretical progress in understanding coherent structures in edge and SOL turbulence," J. Plasma Phys. **74**, 679 (2008).

[8]O. E. Garcia, "Blob transport in the plasma edge: A review," Plasma Fusion Res. **4**, 019 (2009).

[9]D. A. D'Ippolito, J. R. Myra, and S. J. Zweben, "Convective transport by intermittent blob-filaments: Comparison of theory and experiment," Phys. Plasmas **18**, 060501 (2011).

[10]N. Asakura, Y. Koide, K. Itami, N. Hosogan, K. Shimizu, S. Tsuji-Iio, S. Sakurai, and A. Sakasai, "SOL plasma profiles under radiative and detached divertor conditions in JT-60U," J. Nucl. Mater. **241–243**, 559 (1997).

[11]B. LaBombard, R. L. Boivin, M. Greenwald, J. Hughes, B. Lipschultz, D. Mossessian, C. S. Pitcher, J. L. Terry, S. J. Zweben, and Alcator Group, "Particle transport in the scrape-off layer and its relationship to discharge density limit in Alcator C-Mod," Phys. Plasmas **8**, 2107 (2001).

[12]B. Lipschultz, B. LaBombard, C. S. Pitcher, and R. Boivin, "Investigation of the origin of neutrals in the main chamber of Alcator C-Mod," Plasma Phys. Controlled Fusion **44**, 733 (2002).

[13]O. E. Garcia, J. Horacek, R. A. Pitts, A. H. Nielsen, W. Fundamenski, J. P. Graves, V. Naulin, and J. J. Rasmussen, "Interchange turbulence in the TCV scrape-off layer," Plasma Phys. Controlled Fusion **48**, L1 (2005).

[14]D. L. Rudakov, J. A. Boedo, R. A. Moyer, P. C. Stangeby, J. G. Watkins, D. G. Whyte, L. Zeng, N. H. Brooks, R. P. Doerner, T. E. Evans, M. E. Fenstermacher, M. Groth, E. M. Hollmann, S. I. Krasheninnikov, C. J. Lasnier, A. W. Leonard, M. A. Mahdavi, G. R. McKee, A. G. McLean, A. Y. Pigarov, W. R. Wampler, G. Wang, W. P. West, and C. P. C. Wong, "Far SOL transport and main wall plasma interaction in DIII-D," Nucl. Fusion **45**, 1589 (2005).

[15]B. LaBombard, J. W. Hughes, D. Mossessian, M. Greenwald, B. Lipschultz, J. L. Terry, and Alcator C-Mod Team, "Evidence for electromagnetic fluid drift turbulence controlling the edge plasma state in the Alcator C-Mod tokamak," Nucl. Fusion **45**, 1658 (2005).

[16]O. E. Garcia, R. A. Pitts, J. Horacek, A. H. Nielsen, W. Fundamenski, V. Naulin, and J. J. Rasmussen, "Turbulent transport in the TCV SOL," J. Nucl. Mater. **363–365**, 575 (2007).

[17]O. E. Garcia, J. Horacek, R. A. Pitts, A. H. Nielsen, W. Fundamenski, V. Naulin, and J. J. Rasmussen, "Fluctuations and transport in the TCV scrape-off layer," Nucl. Fusion **47**, 667 (2007).

[18]O. E. Garcia, R. A. Pitts, J. Horacek, J. Madsen, V. Naulin, A. H. Nielsen, and J. J. Rasmussen, "Collisionality dependent transport in TCV SOL plasmas," Plasma Phys. Controlled Fusion **49**, B47 (2007).

[19]D. Carralero, G. Birkenmeier, H. W. Müller, P. Manz, P. deMarne, S. H. Müller, F. Reimold, U. Stroth, M. Wischmeier, E. Wolfrum, and ASDEX Upgrade Team, "An experimental investigation of the high density transition of the scrape-off layer transport in ASDEX Upgrade," Nucl. Fusion **54**, 123005 (2014).
[20]D. Carralero, H. W. Müller, M. Groth, M. Komm, J. Adamek, G. Birkenmeier, M. Brix, F. Janky, P. Hacek, S. Marsen, F. Reimold, C. Silva, U. Stroth, M. Wischmeier, E. Wolfrum, ASDEX Upgrade Team, COMPASS Team, and JET-EFDA Contributors, "Implications of high density operation on SOL transport: A multimachine investigation," J. Nucl. Mater. **463**, 123 (2015).
[21]F. Militello, L. Garzotti, J. Harrison, J. T. Omotani, R. Scannell, S. Allan, A. Kirk, I. Lupelli, A. J. Thornton, and MAST Team, "Characterisation of the L-mode scrape off layer in MAST: Decay lengths," Nucl. Fusion **56**, 016006 (2016).
[22]N. Vianello, C. Tsui, C. Theiler, S. Allan, J. Boedo, B. Labit, H. Reimerdes, K. Verhaegh, W. A. J. Vijvers, N. Walkden, S. Costea, J. Kovacic, C. Ionita, V. Naulin, A. H. Nielsen, J. J. Rasmussen, B. Schneider, R. Schrittwieser, M. Spolaore, D. Carralero, J. Madsen, B. Lipschultz, F. Militello, TCV Team, and EUROfusion MST1 Team, "Modification of SOL profiles and fluctuations with line-average density and divertor flux expansion in TCV," Nucl. Fusion **57**, 116014 (2017).
[23]N. Vianello, D. Carralero, C. K. Tsui, V. Naulin, M. Agostini, I. Cziegler, B. Labit, C. Theiler, E. Wolfrum, D. Aguiam, S. Allan, M. Bernert, J. Boedo, S. Costea, H. De Oliveira, O. Fevrier, J. Galdon-Quiroga, G. Grenfell, A. Hakola, C. Ionita, H. Isliker, A. Karpushov, J. Kovacic, B. Lipschultz, R. Maurizio, K. McClements, F. Militello, A. H. Nielsen, J. Olsen, J. J. Rasmussen, T. Ravensbergen, H. Reimerdes, B. Schneider, R. Schrittwieser, E. Seliunin, M. Spolaore, K. Verhaegh, J. Vicente, N. Walkden, W. Zhang, ASDEX Upgrade Team, TCV Team, and EUROfusion MST1 Team, "Scrape-off layer transport and filament characteristics in high-density tokamak regimes," Nucl. Fusion **60**, 016001 (2020).
[24]P. C. Liewer, "Measurements of microturbulence in tokamaks and comparisons with theories of turbulence and anomalous transport," Nucl. Fusion **25**, 543 (1985).
[25]M. Endler, "Turbulent SOL transport in stellarators and tokamaks," J. Nucl. Mater. **266–269**, 84 (1999).
[26]B. A. Carreras, "Plasma edge cross-field transport: Experiment and theory," J. Nucl. Mater. **337**, 315 (2005).
[27]S. J. Zweben, J. A. Boedo, O. Grulke, C. Hidalgo, B. LaBombard, R. J. Maqueda, P. Scarin, and J. L. Terry, "Edge turbulence measurements in toroidal fusion devices," Plasma Phys. Controlled Fusion **49**, S1 (2007).
[28]O. E. Garcia, I. Cziegler, R. Kube, B. LaBombard, and J. L. Terry, "Burst statistics in Alcator C-Mod SOL turbulence," J. Nucl. Mater. **438**, S180 (2013).
[29]O. E. Garcia, S. M. Fritzner, R. Kube, I. Cziegler, B. LaBombard, and J. L. Terry, "Intermittent fluctuations in the Alcator C-Mod scrape-off layer," Phys. Plasmas **20**, 055901 (2013).
[30]O. E. Garcia, J. Horacek, and R. A. Pitts, "Intermittent fluctuations in the TCV scrape-off layer," Nucl. Fusion **55**, 062002 (2015).
[31]A. Theodorsen, O. E. Garcia, J. Horacek, R. Kube, and R. A. Pitts, "Scrape-off layer turbulence in TCV: Evidence in support of stochastic modelling," Plasma Phys. Controlled Fusion **58**, 044006 (2016).
[32]O. E. Garcia, R. Kube, A. Theodorsen, J.-G. Bak, S.-H. Hong, H.-S. Kim, R. A. Pitts, and KSTAR Team, "SOL width and intermittent fluctuations in KSTAR," Nucl. Mater. Energy **12**, 36 (2017).
[33]A. Theodorsen, O. E. Garcia, R. Kube, B. LaBombard, and J. L. Terry, "Relationship between frequency power spectra and intermittent, large-amplitude bursts in the Alcator C-Mod scrape-off layer," Nucl. Fusion **57**, 114004 (2017).
[34]N. R. Walkden, A. Wynn, F. Militello, B. Lipschultz, G. Matthews, C. Guillemaut, J. Harrison, D. Moulton, and JET Contributors, "Statistical analysis of the ion flux to the JET outer wall," Nucl. Fusion **57**, 036016 (2017).
[35]N. R. Walkden, A. Wynn, F. Militello, B. Lipschultz, G. Matthews, C. Guillemaut, J. Harrison, D. Moulton, and JET Contributors, "Interpretation of scrape-off layer profile evolution and first-wall ion flux statistics on JET using a stochastic framework based on filamentary motion," Plasma Phys. Controlled Fusion **59**, 085009 (2017).
[36]R. Kube, O. E. Garcia, A. Theodorsen, D. Brunner, A. Q. Kuang, B. LaBombard, and J. L. Terry, "Intermittent electron density and temperature fluctuations and associated fluxes in the Alcator C-Mod scrape-off layer," Plasma Phys. Controlled Fusion **60**, 065002 (2018).
[37]O. E. Garcia, R. Kube, A. Theodorsen, B. LaBombard, and J. L. Terry, "Intermittent fluctuations in the Alcator C-Mod scrape-off layer for ohmic and high confinement mode plasmas," Phys. Plasmas **25**, 056103 (2018).
[38]A. Theodorsen, O. E. Garcia, R. Kube, B. LaBombard, and J. L. Terry, "Universality of Poisson-driven plasma fluctuations in the Alcator C-Mod scrape-off layer," Phys. Plasmas **25**, 122309 (2018).
[39]A. Bencze, M. Berta, A. Buzás, P. Hacek, J. Krbec, M. Szutyányi, and COMPASS Team, "Characterization of edge and scrape-off layer fluctuations using the fast Li-BES system on COMPASS," Plasma Phys. Controlled Fusion **61**, 085014 (2019).
[40]R. Kube, O. E. Garcia, A. Theodorsen, A. Q. Kuang, B. LaBombard, J. L. Terry, and D. Brunner, "Statistical properties of the plasma fluctuations and turbulent cross-field fluxes in the outboard mid-plane scrape-off layer of Alcator C-Mod," Nucl. Mater. Energy **18**, 193 (2019).
[41]A. Kuang, B. LaBombard, D. Brunner, O. E. Garcia, R. Kube, and A. Theodorsen, "Plasma fluctuations in the scrape-off layer and at the divertor target in Alcator C-Mod and their relationship to divertor collisionality and density shoulder formation," Nucl. Mater. Energy **19**, 295 (2019).
[42]R. Kube, A. Theodorsen, O. E. Garcia, D. Brunner, B. LaBombard, and J. L. Terry, "Comparison between mirror Langmuir probe and gas-puff imaging measurements of intermittent fluctuations in the Alcator C-Mod scrape-off layer," J. Plasma Phys. **86**, 905860519 (2020).
[43]O. E. Garcia, "Stochastic modeling of intermittent scrape-off layer plasma fluctuations," Phys. Rev. Lett. **108**, 265001 (2012).
[44]R. Kube and O. E. Garcia, "Convergence of statistical moments of particle density time series in scrape-off layer plasmas," Phys. Plasmas **22**, 012502 (2015).
[45]A. Theodorsen and O. E. Garcia, "Level crossings, excess times, and transient plasma-wall interactions in fusion plasmas," Phys. Plasmas **23**, 040702 (2016).
[46]O. E. Garcia, R. Kube, A. Theodorsen, and H. L. Pécseli, "Stochastic modelling of intermittent fluctuations in the scrape-off layer: Correlations, distributions, level crossings, and moment estimation," Phys. Plasmas **23**, 052308 (2016).
[47]F. Militello and J. T. Omotani, "Scrape off layer profiles interpreted with filament dynamics," Nucl. Fusion **56**, 104004 (2016).
[48]F. Militello and J. T. Omotani, "On the relation between non-exponential scrape off layer profiles and the dynamics of filaments," Nucl. Fusion **58**, 125004 (2016).
[49]A. Theodorsen and O. E. Garcia, "Statistical properties of a filtered Poisson process with additive random noise: Distributions, correlations and moment estimation," Phys. Scr. **92**, 054002 (2017).
[50]O. E. Garcia and A. Theodorsen, "Auto-correlation function and frequency spectrum due to a super-position of uncorrelated exponential pulses," Phys. Plasmas **24**, 032309 (2017).
[51]A. Theodorsen and O. E. Garcia, "Level crossings and excess times due to a superposition of uncorrelated exponential pulses," Phys. Rev. E **97**, 012110 (2018).
[52]F. Militello, T. Farley, K. Mukhi, N. Walkden, and J. T. Omotani, "A two-dimensional statistical framework connecting thermodynamic profiles with filaments in the scrape off layer and application to experiments," Phys. Plasmas **25**, 056112 (2018).
[53]A. Theodorsen and O. E. Garcia, "Probability distribution functions for intermittent scrape-off layer plasma fluctuations," Plasma Phys. Controlled Fusion **60**, 034006 (2018).
[54]P. W. Terry, M. Greenwald, J.-N. Leboeuf, G. R. McKee, D. R. Mikkelsen, W. M. Nevins, D. E. Newman, D. P. Stotler, Task Group on Verification and Validation, U.S. Burning Plasma Organization, and U.S. Transport Task Force, "Validation in fusion research: Towards guidelines and best practices," Phys. Plasmas **15**, 062503 (2008).
[55]M. Greenwald, "Verification and validation for magnetic fusion," Plasma Phys. Controlled Fusion **17**, 058101 (2010).
[56]C. Holland, "Validation metrics for turbulent plasma transport," Phys. Plasmas **23**, 060901 (2016).

[57]G. Decristoforo, A. Theodorsen, and O. E. Garcia, "Intermittent fluctuations due to Lorentzian pulses in turbulent thermal convection," Phys. Fluids **32**, 085102 (2020).
[58]O. Pogutse, W. Kerner, V. Gribkov, S. Bazdenkov, and M. Osipenko, "The resistive interchange convection in the edge of tokamak plasmas," Plasma Phys. Controlled Fusion **36**, 1963 (1994).
[59]H. Sugama and W. Horton, "L-H confinement mode dynamics in three-dimensional state space," Plasma Phys. Controlled Fusion **37**, 345 (1995).
[60]P. Beyer and K. H. Spatschek, "Center manifold theory for the dynamics of the L-H-transition," Phys. Plasmas **3**, 995 (1996).
[61]W. Horton, G. Hu, and G. Laval, "Turbulent transport in mixed states of convective cells and sheared flows," Phys. Plasmas **3**, 2912 (1996).
[62]M. Berning and K. H. Spatschek, "Bifurcations and transport barriers in the resistive-g paradigm," Phys. Rev. E **62**, 1162 (2000).
[63]O. E. Garcia, N. H. Bian, J.-V. Paulsen, S. Benkadda, and K. Rypdal, "Confinement and bursty transport in a flux-driven convection model with sheared flows," Plasma Phys. Controlled Fusion **45**, 919 (2003).
[64]O. E. Garcia and N. H. Bian, "Bursting and large-scale intermittency in turbulent convection with differential rotation," Phys. Rev. E **68**, 047301 (2003).
[65]O. E. Garcia, N. H. Bian, V. Naulin, A. H. Nielsen, and J. J. Rasmussen, "Two-dimensional convection and interchange motions in fluids and magnetized plasmas," Phys. Scr. **2006**(T122), 104.
[66]F. Wilczynski, D. W. Hughes, S. V. Loo, W. Arter, and F. Militello, "Stability of scrape-off layer plasma: A modified Rayleigh–Bénard problem," Phys. Plasmas **26**, 022510 (2019).
[67]S. Benkadda, X. Garbet, and A. Verma, "Interchange instability turbulence model in edge tokamak plasma," Contrib. Plasma Phys. **34**, 247 (1994).
[68]O. E. Garcia, "Two-field transport models for magnetized plasmas," J. Plasma Phys. **65**, 81 (2001).
[69]Y. Sarazin and P. Ghendrih, "Intermittent particle transport in two-dimensional edge turbulence," Phys. Plasmas **5**, 4214 (1998).
[70]P. Ghendrih, Y. Sarazin, G. Attuel, S. Benkadda, P. Beyer, G. Falchetto, C. Figarella, X. Garbet, V. Grandgirard, and M. Ottaviani, "Theoretical analysis of the influence of external biasing on long range turbulent transport in the scrape-off layer," Nucl. Fusion **43**, 1013 (2003).
[71]Y. Sarazin, P. Ghendrih, G. Attuel, C. Clément, X. Garbet, V. Grandgirard, M. Ottaviani, S. Benkadda, P. Beyer, N. Bian, and C. Figarella, "Theoretical understanding of turbulent transport in the SOL," J. Nucl. Mater. **313**, 796 (2003).
[72]O. E. Garcia, V. Naulin, A. H. Nielsen, and J. J. Rasmussen, "Computations of intermittent transport in scrape-off layer plasmas," Phys. Rev. Lett. **92**, 165003 (2004).
[73]O. E. Garcia, V. Naulin, A. H. Nielsen, and J. J. Rasmussen, "Turbulence and intermittent transport at the boundary of magnetized plasmas," Phys. Plasmas **12**, 062309 (2005).
[74]O. E. Garcia, V. Naulin, A. H. Nielsen, and J. J. Rasmussen, "Turbulence simulations of blob formation and radial propagation in toroidally magnetized plasmas," Phys. Scr. **2006**(T122), 89.
[75]J. R. Myra, D. A. Russell, and D. A. D'Ippolito, "Transport of perpendicular edge momentum by drift-interchange turbulence and blobs," Phys. Plasmas **15**, 032304 (2008).
[76]D. A. Russell, J. R. Myra, and D. A. D'Ippolito, "Saturation mechanisms for edge turbulence," Phys. Plasmas **16**, 122304 (2009).
[77]J. R. Myra, W. M. Davis, D. A. D'Ippolito, B. LaBombard, D. A. Russell1, J. L. Terry, and S. J. Zweben, "Edge sheared flows and the dynamics of blob-filaments," Nucl. Fusion **53**, 073013 (2013).
[78]N. Bisai, A. Das, S. Deshpande, R. Jha, P. Kaw, A. Sen, and R. Singh, "Simulation of plasma transport by coherent structures in scrape-off-layer tokamak plasmas," Phys. Plasmas **11**, 4018 (2004).
[79]N. Bisai, A. Das, S. Deshpande, R. Jha, P. Kaw, A. Sen, and R. Singh, "Edge and scrape-off layer tokamak plasma turbulence simulation using two-field fluid model," Phys. Plasmas **12**, 072520 (2005).
[80]N. Bisai, A. Das, S. Deshpande, R. Jha, P. Kaw, A. Sen, and R. Singh, "Formation of a density blob and its dynamics in the edge and the scrape-off layer of a tokamak plasma," Phys. Plasmas **12**, 102515 (2005).
[81]A. H. Nielsen, G. S. Xu, J. Madsen, V. Naulin, J. J. Rasmussen, and B. N. Wan, "Simulation of transition dynamics to high confinement in fusion plasmas," Phys. Lett. A **379**, 3097 (2015).
[82]A. H. Nielsen, J. J. Rasmussen, J. Madsen, G. S. Xu, V. Naulin, J. M. B. Olsen, M. Løiten, S. K. Hansen, N. Yan, L. Tophøj, and B. N. Wan, "Numerical simulations of blobs with ion dynamics," Plasma Phys. Controlled Fusion **59**, 025012 (2017).
[83]J. Olsen, A. H. Nielsen, J. J. Rasmussen, J. Madsen, T. Eich, B. Sieglin, and V. Naulin, "Scrape-off layer power fall-off length from turbulence simulations of ASDEX Upgrade L-mode," Plasma Phys. Controlled Fusion **60**, 085018 (2018).
[84]B. Dudson, M. Umansky, X. Xu, P. Snyder, and H. Wilson, "BOUT++: A framework for parallel plasma fluid simulations," Comput. Phys. Commun. **180**, 1467 (2009).
[85]F. Militello, B. Dudson, L. Easy, A. Kirk, and P. Naylor, "On the interaction of scrape off layer filaments," Plasma Phys. Controlled Fusion **59**, 125013 (2017).
[86]G. D. Byrne and A. C. Hindmarsh, "PVODE, an ODE solver for parallel computers," Int. J. High Perform. Comput. Appl. **13**, 354 (1999).
[87]J. E. Maggs and G. J. Morales, "Generality of deterministic chaos, exponential spectra, and Lorentzian pulses in magnetically confined plasmas," Phys. Rev. Lett. **107**, 185003 (2011).
[88]O. E. Garcia and A. Theodorsen, "Power law spectra and intermittent fluctuations due to uncorrelated Lorentzian pulses," Phys. Plasmas **24**, 020704 (2017).
[89]O. E. Garcia and A. Theodorsen, "Skewed Lorentzian pulses and exponential frequency power spectra," Phys. Plasmas **25**, 014503 (2018).
[90]O. E. Garcia and A. Theodorsen, "Intermittent fluctuations due to uncorrelated Lorentzian pulses," Phys. Plasmas **25**, 014506 (2018).
[91]G. Decristoforo, F. Militello, T. Nicholas, J. Omotani, C. Marsden, N. Walkden, and O. E. Garcia, "Blob interactions in 2D scrape-off layer simulations," Phys. Plasmas **27**, 122301 (2020).
[92]F. D. Halpern, P. Ricci, S. Jolliet, J. Loizu, J. Morales, A. Mosetto, F. Musil, F. Riva, T. M. Tran, and C. Wersal, "The GBS code for tokamak scrape-off layer simulations," J. Comput. Phys. **315**, 388 (2016).
[93]P. Tamain, H. Bufferand, G. Ciraoloa, C. Colin, D. Galassi, P. Ghendrih, and F. Schwander, "The TOKAM3X code for edge turbulence fluid simulations of tokamak plasmas in versatile magnetic geometries," J. Comput. Phys. **321**, 606 (2016).
[94]B. D. Dudson and J. Leddy, "Hermes: Global plasma edge fluid turbulence simulations," Plasma Phys. Controlled Fusion **59**, 054010 (2017).
[95]M. Held, M. Wiesenberger, R. Kube, and A. Kendl, "Non-Oberbeck–Boussinesq zonal flow generation," Nucl. Fusion **58**, 104001 (2018).
[96]M. Wiesenberger, L. Einkemmer, M. Held, A. Gutierrez-Milla, X. Sáez, and R. Iakymchuk, "Reproducibility, accuracy and performance of the FELTOR code and library on parallel computer architectures," Comput. Phys. Commun. **238**, 145 (2019).
[97]A. Stegmeir, A. Ross, T. Body, M. Francisquez, W. Zholobenko, D. Coster, F. Jenko, B. N. Rogers, and K. S. Kang, "Global turbulence simulations of the tokamak edge region with GRILLIX," Phys. Plasmas **26**, 052517 (2019).
[98]D. R. Zhang, Y. P. Chen, X. Q. Xu, and T. Y. Xia, "Self-consistent simulation of transport and turbulence in tokamak edge plasma by coupling SOLPS-ITER and BOUT++," Phys. Plasmas **26**, 012508 (2019).
[99]D. A. Russell, J. R. Myra, and D. P. Stotler, "A reduced model of neutral-plasma interactions in the edge and scrape-off-layer: Verification comparisons with kinetic Monte Carlo simulations," Phys. Plasmas **26**, 022304 (2019).
[100]M. Giacomin and P. Ricci, "Investigation of turbulent transport regimes in the tokamak edge by using two-fluid simulations," J. Plasma Phys. **86**, 905860502 (2020).